Chaos in an Imperfectly Premixed Model Combustor

Lipika Kabiraj,[1, a)] Aditya Saurabh,[1] Nader Karimi,[2] Anna Sailor,[3] Epaminondas Mastorakos,[4] Ann P. Dowling,[4] and Christian O. Paschereit[1]
[1)] *Hermann Föttinger Institute, Technische Universität Berlin, Germany.*
[2)] *School of Engineering, University of Glasgow, UK*
[3)] *University of Wisconsin-Madison, Madison, USA*
[4)] *Department of Engineering, University of Cambridge, UK*

(Dated: 16 January 2015)

This article reports nonlinear bifurcations observed in a laboratory scale, turbulent combustor operating under imperfectly premixed mode with global equivalence ratio as the control parameter. The results indicate that the dynamics of thermoacoustic instability correspond to quasi-periodic bifurcation to low-dimensional, deterministic chaos, a route that is universal to the class of dissipative nonlinear systems. The results support the recent identification of universal bifurcation behavior in a laminar premixed flame combustor (Kabiraj et al., Chaos 22, 2012) and extend the observation to a practically relevant combustor configuration.

PACS numbers: Valid PACS appear here
Keywords: Thermoacoustic instabilities, Nonlinear oscillations, Imperfectly premixed flame, Chaos

Spontaneous feedback coupling between the flame and chamber acoustics in a combustor can have disastrous consequences. Hence, thermoacoustic instability, as this phenomenon is technically referred to, is a critical issue for industries dependent on combustor technology. Thermoacoustic instability also is an interesting case of nonlinear time-delayed coupling. A recent development in the research on thermoacoustic instability is the identification of chaotic dynamics and chaotic scenarios in simple model combustors running on laminar flames. As the flame is an inherent part of the instability, one could expect clean chaotic transitions to be specific to simple laminar systems. We will show here that this is not the case. This article is a report on the nonlinear analysis of thermoacoustic instability in a more realistic combustor configuration. We conducted experiments on a combustor operating on imperfectly premixed, turbulent combustion with equivalence ratio as the control parameter for bifurcation analysis. Imperfectly premixed combustion is the preferred mode of operation in real systems due to its advantages over the premixed mode. Of the several variables in a combustor, the fuel-air or equivalence ratio is the most likely to vary. We calculate and analyze dynamical measures of chaos and complexity from the phase space reconstructed from experimental data while varying the control parameter. Results demonstrate that a well-defined route to chaos is followed by the instability in the combustor even in the presence of several complexities that are absent in laminar flame combustors. The main development over recent results that this article presents is to demonstrate that even in a practical configuration, the thermoacoustic system exhibits deterministic chaotic dynamics and a well-defined route to chaos, which has been observed in several other nonlinear systems. These results uncover a new aspect of the instability and will motivate the incorporation of new approaches based on dynamical systems theory for the modeling and control of thermoacoustic instability. The study also introduces a naturally occurring phenomenon that is of technical relevance to the class of nonlinear systems exhibiting rich dynamics.

I. INTRODUCTION

Stable operation is an essential requirement for any practical system. Industrial combustors such as those employed in gas turbine engines and furnaces are no exceptions to this requirement. Thermoacoustic instability is one of the major issues that disrupt stable operation in combustors[1]. The spontaneously excited and self-sustained acoustic and heat release rate oscillations that arise in the system at the onset of the instability cause an undesirable and abrupt increase in the mechanical as well as thermal loading on the structural components of the combustor. In extreme cases, the structural integrity of the entire system can be adversely affected. These effects, in turn, result in problems such as increased maintenance requirements, a decreased life-span of the system and in the worst case, complete system failure. To address this critical issue, fundamental and applied research on understanding the phenomenon is presently being actively pursued.

In simple terms, thermoacoustic instability is caused by heat release fluctuations coupled with acoustic oscillations in the combustion zone[2]. Lord Rayleigh was the first to postulate a phenomenological description[3] of the coupling: growth in acoustic energy is positive

[a)] Electronic mail: lipika.kabiraj@tu-berlin.de

if acoustic oscillations at the flame and unsteady heat release oscillations are in phase with each other. To elaborate, fluctuations in a typical flame generate fluctuations in the heat release rate. This unsteady heat release rate generates acoustic fluctuations that reflect from the acoustic boundaries of the combustor and provide additional perturbation to the flame. If the Rayleigh criterion is satisfied, a constructive feedback loop gets established and these thermoacoustic oscillations are amplified. As acoustic damping processes are always present in the system, instabilities will occur when amplification in acoustic oscillations due to the feedback coupling exceeds acoustic damping. At first, the oscillation amplitude grows exponentially. But, beyond a certain amplitude, nonlinear mechanisms that are associated primarily with the flame come into play. Saturation of the flame response is one of the nonlinear effects; it results in a balance between amplification and damping of acoustic energy. The dynamics of self-excited oscillations are governed by nonlinear interactions in the system.

Our analysis in this paper is based on a model combustor configuration that features characteristic properties of a practical systems: highly turbulent flow conditions, presence of hydrodynamic instabilities, and, an imperfectly premixed flame. We elaborate on the last feature as it will help in providing a description of the test setup. In a perfectly premixed combustors, fuel and air are introduced such that a uniform reactant mixture reaches the flame. To achieve this, air and fuel are mixed at a point far upstream of the dump plane, so that the mixture has a long mixing length. However, in such a configuration, flashback is a serious concern due to the existence of combustible air and fuel mixture inside the plenum chamber. In the imperfectly premixed case, however, the reactant composition is spatially and temporally non-uniform and the plenum consists only of air. This is because under imperfectly premixed conditions fuel is introduced into the chamber much close to the combustion zone and has less time to mix with air. As flashback in not an issue, there is a practical interest in imperfectly premixed flames from the viewpoint of safety and reliability. But this configuration brings an additional variable the phenomenon of thermoacoustic instability: equivalence ratio fluctuations. Equivalence ratio oscillations are known to participate in thermoacoustic coupling[4–6].

Moving to the current state of research on thermoacoustic instability, over the past few decades, investigations on thermoacoustic instabilities have generated extensive literature on the phenomenon (see Refs. 1, 2, and 7 for reviews covering major developments). Various direct and indirect mechanisms that are associated with thermoacoustic instability have been identified. It has been found that the primary factors that lead to oscillations in unsteady heat release rate during thermoacoustic instability are oscillations at the burner inlet velocity and equivalence ratio oscillations. Individual contribution of the two has been investigated by studying the response of premixed and partially-premixed flames to velocity and equivalence ratio fluctuations[8–13]. As often the direct and indirect mechanisms of flame response are inherently coupled, it has been difficult to isolate individual contributions. However, such investigations have provided critical understanding on the dynamics of flame response.

Hence, most of the attempts in characterizing flame dynamics have been, so far, around the notion of flame transfer function[7,13,14]. Inspired by the linear control theory, in this method the flame response to low amplitude single frequency disturbances is determined in an uncoupled system. The experiment is repeated for a wide range of forcing frequencies to evaluate the flame frequency response[11]. The resultant transfer function can be included in a network model of system acoustics to develop a predictive thermo-acoustic model of the combustor[13,14]. This model can be then used to predict the stability and state of the pressure and heat release fluctuations[1,14].

In recent developments this method has been extended to study the non-linear flame dynamics. The extension is called the flame describing function[12,15–18]. The latter takes both frequency and amplitude of excitation as the inputs and is therefore a nonlinear characterization of the flame response[19]. In addition to inlet velocity disturbances, nonlinear flame response to equivalence ratio oscillations has also been studied[20–22]. Studies on nonlinear flame response to velocity oscillations indicate nonlinearity in the flame response arises from kinematic mechanisms such as vortex roll-up, pinching, cusp formation and flame lift-up. While studies on flame response to equivalence ratio fluctuations indicate that mechanisms such as flame stretch effects; variation in heat of reaction, flame speed; and indirect influence of flame surface area, determine the nonlinear flame response. Both branches of flame response investigation indicate that the flame is a highly nonlinear element.

In addition to flame response studies, recent developments have also emphasized the importance of investigating the nonlinear dynamics of the coupled thermoacoustic system (see Refs. 23–27). These studies on self-excited nonlinear thermoacoustic oscillations show that thermoacoustic systems can exhibit quite a rich variety of nonlinear behavior. Such investigations of the coupled system provide the opportunity to study the full spectrum of the nonlinear characteristics of thermoacoustic oscillations. This paper goes in the direction of these recent developments on the study of self-excited nonlinear thermoacoustic oscillations. We investigate nonlinear bifurcations in a model lean, imperfectly premixed flame combustor. We follow a dynamical systems approach to characterize dynamical states and bifurcations obtained in the experiments. We have observed that even in the complex configuration investigated, the nonlinear dynamics of thermoacoustic oscillations correspond to fundamental low-dimensional nonlinear systems.

The contents that follow in this article are divided into four main sections. A short theoretical background on

concepts and methods employed in this article are discussed next. This section also contains a more detailed account of recent findings on the nonlinear dynamics of thermoacoustic systems. The description of the experimental setup follows next. After these preliminaries we present the main results and discussions of our study. We then conclude with a short summary of our study.

II. THEORETICAL BACKGROUND

This section presents a brief overview of select concepts from the dynamical systems theory that are relevant to the results and discussions presented in Sec. IV.

Natural phenomena, such as thermoacoustic instability, are inherently nonlinear. This implies that the temporal/dynamical evolution of such systems is governed by laws that are nonlinear. A distinguishing feature of such nonlinear evolution is the property called *bifurcation*: changes in a critical system parameter result in characteristic changes in the temporal dynamics of the system. These bifurcations that occur at critical points with respect to the control parameter, together with the characteristics of dynamical states that are involved, describe how the system loses its stability with variation in the critical parameter. It is known that bifurcations exhibited in unrelated nonlinear systems can be qualitatively identical. And therefore, bifurcations are classified into generic types. It is an obvious advantage if the dynamics of the nonlinear system under investigation can be related to a known bifurcation behavior. In the theory of nonlinear systems, bifurcation theory and bifurcation analysis are central themes.

It can be noted that, particularly in experimental investigations, the analysis of bifurcations provides critical insights into the nature and properties of the governing equations that might be unknown apriori. Information on how to improve existing system models could also be derived from the results of bifurcation analysis. Furthermore, to understand the physics underlying the investigated system, one would benefit from a comparison of system dynamics, in particular, bifurcation and the resulting states, with various known dynamical systems.

A. Bifurcations, Bifurcation Scenarios and Chaos

As mentioned, bifurcations have been classified on the basis of dynamical changes that occur in nonlinear system with varying control parameters. Regarding the case presented here, the Hopf bifurcation is of importance. At a Hopf bifurcation, bifurcation from a steady state to steady periodic oscillations—a limit cycle— takes place. This implies that, in the frequency spectrum, one would find the emergence of a peak at the frequency of oscillation.

It is important to note that a nonlinear system can undergo successive bifurcations after the primary bifurcation. After multiple successive bifurcations that lead to increasingly complex dynamics, the system may undergo transition to deterministic chaos[28]. Chaos has been found to be ubiquitous in nonlinear systems[28]. It is a specific dynamical state characterized by an exponential separation between trajectories that start from neighboring points in the phase space[28]. Often the geometry of the chaotic attractor is a fractal object, characterized by a non-integer dimension.

It has been observed that almost all known cases of the loss of stability and subsequent transition to chaos of a nonlinear systems can be accounted for by a small set of bifurcation sequences. These specific series of bifurcations are referred to as scenarios or routes to chaos.

In order to proceed with bifurcation analysis, appropriate methods are required to characterize the dynamical states. The conventional methods, often used in the thermoacoustic community, such as the power spectrum, are quite helpful. However, for instance for cases like chaos, where the spectrum acquires properties similar to the time series of a stochastic process, the spectral analysis is clearly not a suitable method. Changes in system dynamics due to a bifurcation are reflected as qualitative changes in the phase space attractor. Therefore, phase space based methods are appropriate for characterization of system dynamics, and therefore, bifurcations. The two phase space based measures used here for quantitative characterization of attractors— particularly for quantifying the degree of complexity and chaos in the attractor— are the attractor dimension and the Lyapunov exponent.

At this stage it is clear that we require a method to obtain the phase space from thermoacoustic data acquired in our experiments. Time-delay embedding is a well-established method of reconstruction of the phase space from scalar measurements[29] and is employed in this article for the analysis of results.

B. Phase space reconstruction

Phase space reconstruction based on time-delay embedding comprises of extracting time-delayed vectors from the time trace and using these as substitutes for phase space coordinates. Given a scalar time series, such as the pressure time trace, acquired at discrete time steps, $p_i = p(t_0 + i\tau_s)$, with τ_s as the sampling time interval, a set of time-delayed vectors define the reconstructed phase space:

$$\mathbf{x}_i = \{p_i, p_{i+\tau_d}, p_{i+2\tau_d}, \ldots, p_{i+(m-1)\tau_d}\}. \qquad (1)$$

A proper reconstruction which can be employed for subsequent analysis depends on the choice of the time delay, τ_d and the embedding dimension, m. Here, we chose the average mutual information and false nearest neighbor methods for the calculation of the optimum time delay and the embedding dimension[30] respectively.

C. Attractor dimension

The correlation dimension, $\mathbf{D}_2$[31] is used as the measure of the attractor dimension here. The estimation of $\mathbf{D}_2$ is based on the Grassberger-Procassia method[32]. This measure is an invariant property of the attractor and can be obtained from the reconstructed phase space trajectory. The attractor correlation dimension is given by,

$$\lim_{N\to\infty}\lim_{\epsilon\to\infty}\mathbf{D}_2 = \frac{\log(C^N(m,\epsilon))}{\log(\epsilon)}, \text{with} \tag{2}$$

$$C^N(m,\epsilon) = \frac{1}{N}\sum_i C_i, \tag{3}$$

$$C_i = \frac{1}{N}\sum_j \Theta\left|\mathbf{x}_i - \mathbf{x}_j\right|, \tag{4}$$

where N is the number of phase space points, Θ is the Heaviside function and $|\cdot|$ denotes the Euclidean norm. Problems arise in experimentally acquired data as the two limits cannot be satisfied. However, a robust estimate can still be obtained with attention to pitfalls associated with the estimation on the basis of reconstructed attractors.

The dimension is an indication of the number of degrees of freedom active in the system for a given parameter. For the complex case of chaotic dynamics, the attractor is often known to exhibit fractal properties. Accordingly, $\mathbf{D}_2$ for chaotic attractors is a non-integer.

D. Lyapunov exponent

It is a characteristic property of a chaotic attractor that neighbouring trajectories diverge with respect to each other with time. This property can also be interpreted as a sensitive dependence of the system evolution with the initial conditions—famously the Butterfly effect. In this article, this property is used as a basis for the characterization of dynamical states and detection the transition to chaos. Specifically, we use the method proposed in Kantz[30] for the estimation of the maximal Lyapunov exponent, λ_{max}:

$$S(\tau) = \frac{1}{T}\sum_{t=1}^{T}\ln\left(\frac{1}{|\mathcal{U}_t|}\sum_{i\in\mathcal{U}_t} dist\left(\mathbf{x}_t,\mathbf{x}_i;\tau\right)\right), \tag{5}$$

where $\mathcal{U}_t$ is the neighborhood of any point $\mathbf{x}_t$ in the phase space and $dist(\mathbf{x}_t,\mathbf{x}_i;\tau)$ is defined as

$$dist(\mathbf{x}_t,\mathbf{x}_i;\tau) = |x_{t+\tau} - x_{i+\tau}| \tag{6}$$

The quantity $S(\tau)$ scales linearly with τ in an intermediate range with a slope corresponding to the maximal Lyapunov exponent. Further details about the algorithm and its implementation on experimentally acquired time series data can be found in Kantz[30], Kantz and Schreiber[33]. A positive value of λ_{max} is an indication of chaotic dynamics. The algorithm is also robust against noise.

E. Bifurcations/Chaos in Thermoacoustic Systems

It is well recognized that thermoacoustic instability is a result of either a subcritical or a supercritical Hopf bifurcation. On account of the importance of Hopf bifurcations in thermoacoustic systems, it has been extensively studied previously in the context of the stability border of thermoacoustic systems[34,35].

The identification of nonlinear bifurcations leading to chaos, however, can be considered a relatively recent development in the field of thermoacoustic instability. Recent experimental reports include Kabiraj et al.[23] and Gotoda et al.[24]. Numerical simulation of bifurcations to chaos on a model thermoacoustic system was reported by Kashinath et al.[27]. While Gotoda et al.[24] established the presence of deterministic chaos, well-defined routes to chaos: Ruelle-Takens-Newhouse and the intermittency route, were identified in experiments on a laminar premixed combustors with flame location as the control parameter in Kabiraj et al.[23] and Kabiraj & Sujith[36]. In this paper, we demonstrate that even in a practically relevant configuration of a turbulent combustor operated under imperfectly premixed conditions, chaos and a universal bifurcation scenario determines system dynamics.

III. EXPERIMENTAL SETUP

The set of experiments were performed on a 10 kW small-scale combustor, detailed in Figure 1. The same setup was used by Karimi et. al [37], and was employed for the observation of nonlinear flame response to acoustic velocity fluctuations at the burner inlet by Balachandran et al., [18]. In its simplest form, the combustor included a 300 mm long circular duct of inner diameter of 35 mm with a conical bluff-body of diameter 25 mm. This resulted in a blockage ratio of 50% which stabilized the flame. To further improve flame stabilization, a flow swirler with a swirl angle of 60 degrees was placed 45 mm upstream of the bluff-body edge. The cold gases flow through a 200 mm long plenum chamber of inner diameter 100 mm. The plenum and duct contain a few layers of flow straightener to produce a uniform flow. The downstream flame confinement consisted of a section with inner diameter of 70 mm of combined brass tubing and a 200 mm long section of quartz tube, making the total length of 510 mm. This duct was open to the atmosphere at the top end.

Fuel was fed into the combustor through the bottom end of the tube supporting the bluff-body (see Fig. 1), while air entered through the plenum chamber. Air and fuel flows were regulated by Alicat Scientific mass flow controllers with the maximum flow rates of 1500 and 100

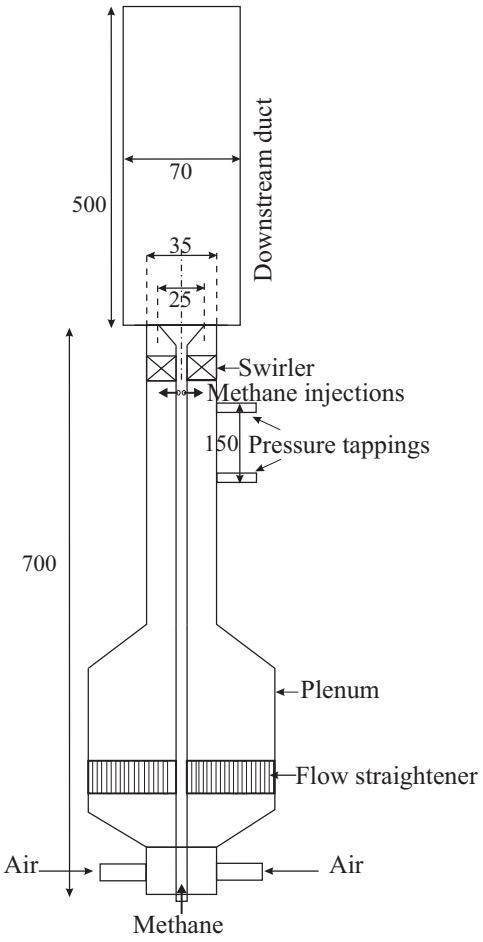

FIG. 1. Schematic of combustion test rig.

standard liters per minute for air and methane respectively, and 1% full scale accuracy. Gaseous methane was injected at a location 55 mm upstream of the bluff body edge (see Fig. 1). This included six holes each with diameter of 250 μm, evenly spaced around the circumference of the tube. Choked methane flows injected at this site close to the reactive region have little time to mix with air injected far upstream, creating an imperfectly premixed condition. For this experiment, a flow velocity of 10 m s^{-1} was maintained at the edge of the bluff-body. The net mass flow rate was adjusted such that changing equivalence ratio values had no effect on this velocity. Thermoacoustic instabilities were observed at the overall equivalence ratios, ϕ, of 0.70 and greater.

Two microphones were set up 150 mm away from each other further upstream of the flame to measure pressure fluctuations in the fuel chamber (Kulite model number XCS093, maximum pressure of 5 psi). The resultant voltage signals were amplified and digitized at sampling rate of 16384 Hz. They were subsequently recorded using LabVIEW. Acquisition of pressure measurements was started at least 90 seconds after the flame ignition and pressure transducer signals were acquired for the periods of 10 seconds.

IV. RESULTS AND DISCUSSION

Experiments were carried out for bifurcation analysis with the equivalence ratio as the control parameter. The value of the overall equivalence ratio was varied in the range $\phi = 0.70$–0.80. Below $\phi = 0.70$, the system was found to be statically unstable (lean blowout). At all measured conditions, pressure oscillations within the combustor were observed to be unsteady. The term unsteady is used to indicate fluctuations that do not pertain to any particular dynamical state. Such fluctuations arise from unavoidable fluctuations in relevant system parameters due to factors such as a high degree of turbulence, hydrodynamic fluctuations and fluctuations in the fuel and air supply. Although the resulting unsteadiness belongs to system dynamics, it is specific to the experiment. Such unsteadiness is observed as relatively large modulation of the signal amplitude. It is not related to dynamical features of thermoacoustic coupling and related bifurcations that is of interest presently. For the convenience of nonlinear analysis, we will isolate the section of the time series where relatively steady oscillations are observed. In subsequent analyses, results have been obtained from such sections of the time trace, unless noted otherwise. In addition, results such as phase portraits, spectra etc. have been presented only for the representative cases for each type of the observed dynamical behavior.

The results in the following describe qualitative as well as quantitative dynamical features of the system at different values of the bifurcation parameter. Details of quantitative characterization through estimates of the correlation dimension and the Lyapunov exponent that are provided towards the end of results and discussions, in Secs. IV D and IV F respectively, support inferences that we make in the following sections.

A. Limit cycle oscillations

The combustor is found to be spontaneously unstable at $\phi = 0.70$, the lowest equivalence ratio investigated. Figure 2 contains the four main plots that provide detailed information on the system dynamics. The plots represent system dynamics for $\phi \in [0.70, 0.75)$. The temporal behavior and the spectral content of the signal is shown in the first two plots on the top row. The spectrum contains a single peak at $f = 335$ Hz. The time series illustrates unsteady oscillations as opposed to steady oscillations with a constant amplitude. Accordingly, the spectrum also shows a broadband nature.

The third plot is a two-dimensional projection ($p(t)$ against $p(t+\tau_d)$) of the reconstructed phase space. From mutual information and nearest neighbor calculations, the optimum time-delay and the optimum embedding dimension were found to be $\tau_d = 12$ and $m = 5$ respectively. The structure is a single loop broadened due to noise. Evidence for the presence of noise rather than deterministic chaos resulting in the broadband spectrum is

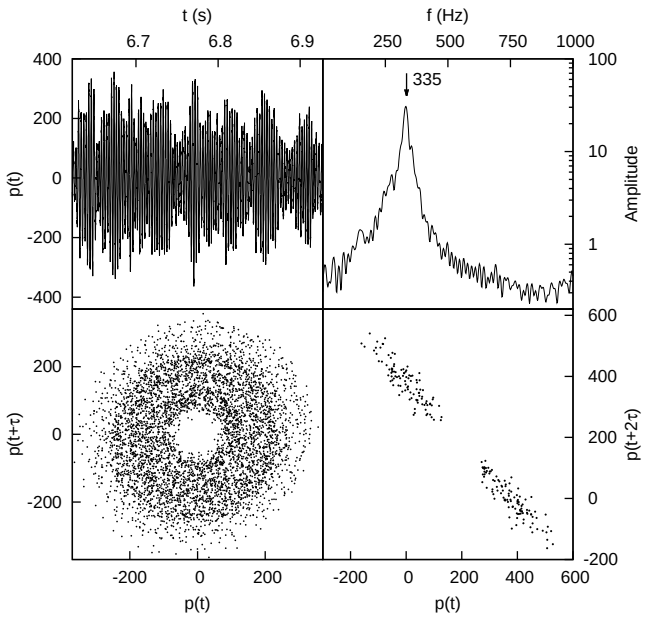

FIG. 2. Limit cycle oscillations at $\phi = 0.70$. Clockwise from top-left: time-trace, power spectrum, 2-d projection of phase space points using the first two delay coordinates, double-sided Poincaré section of the phase portrait.

presented through the estimation of divergence of nearby trajectories in Sec.IV F.

The fourth plot is the Poincaré plot. The Poincaré plot contains points at the intersection between the phase space trajectory and a (Poincaré) plane. An appropriate location of the plane in the phase space is chosen in order to obtain details of the structure of the attractor[38]. The double-sided Poincaré section corresponding to the phase portrait elucidates the presence of a limit cycle. Scattered points on the Poincaré sections indicate noisy limit cycle behavior. Further characterization on the basis of dimension estimates in Sec.IV D supports the argument that the phase space structure is a noisy loop representing a limit cycle.

B. Birth of the two-torus

At $\phi = 0.75$, the first indication of quasi-periodic behavior is identified in the dynamical analysis of the system. For a noisy system such as the turbulent combustor under investigation, quasi-periodicity is clearly observed when a second incommensurate frequency attains a significant amplitude with respect to the frequency in the system after the first Hopf-bifurcation. When this condition is met, the toroidal structure opens enough to distinguish itself from the random excursions of the trajectory due to noise. Figure 3 provides the same details on the dynamics of the system as in Fig. 2 for the overall equivalence ratio, $\phi = 0.78$. The incommensurate frequency associated with quasi-periodicity, noted from the spectrum in Fig. 3, is 265 Hz.

The 2-d projection of the quasiperiodic attractor ($\tau_d = 12, m = 5$) appears to be quite similar to the limit cycle phase portrait. However, its hollow toroidal structure becomes very clear in the Poincaré section.

As the control parameter, the equivalence ratio, is varied, the relative contribution of the new incommensurate frequency varies. Accordingly, the structure of the quasi-periodic torus also changes in the phase space. At $\phi = 0.75$ (not shown here), the quasiperiodic rings in the Poincaré section are small in diameter. As the second incommensurate frequency grows in amplitude, the rings grow in size. In the power spectrum, indications of a third frequency unrelated to the two frequencies of the quasi-periodic state is seen. Contribution from this frequency is related to the next bifurcation. We also note that the first frequency has shifted itself to a higher value of $f = 375$Hz. This is expected due to the increase in the average temperature of the combustor as equivalence ratio increases. The other frequencies present are a linear combination of the two dominant frequencies[39].

C. Torus breaking and chaos

Further increase in the equivalence ratio results in an interesting development. The quasi-periodic torus undergoes breakdown. The state that emerges as a result of this development is chaotic, as we will see from further characterization in Secs. IV D and IV F. The state is characterized by a rich frequency spectrum consisting

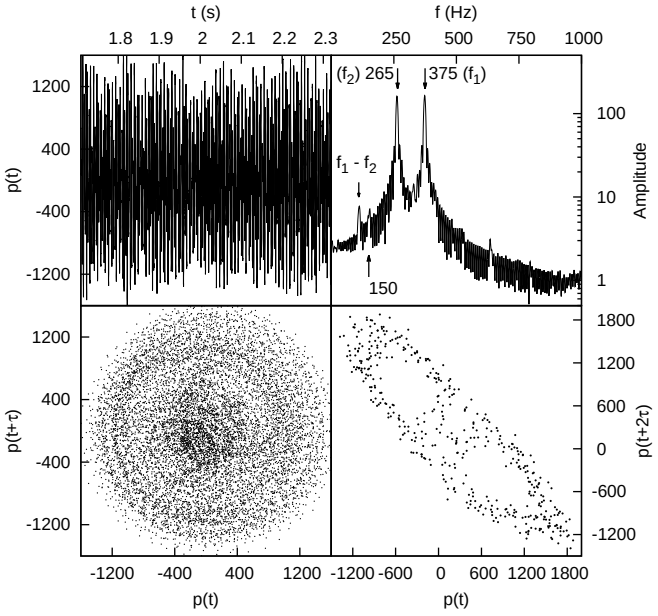

FIG. 3. Quasi-periodic oscillations at $\phi = 0.78$. Clockwise from top-left: time-trace, power spectrum, 2-d projection of phase space points using the first two delay coordinates, double-sided Poincaré section of the phase portrait.

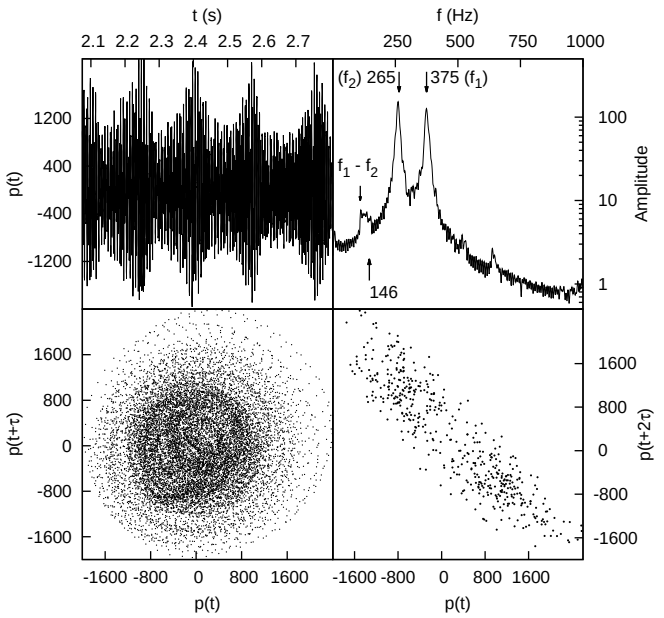

FIG. 4. Chaotic oscillations at $\phi = 0.79$. Clockwise from top-left: time-trace, power spectrum, 2-d projection of phase space points using the first two delay coordinates, double-sided Poincaré section of the phase portrait.

of multiple observable broadband peaks (Fig. 4). We note that the emergence of this state is accompanied by a contribution of the third frequency at 146 Hz. The new frequency causes the quasi-periodic torus to destabilize and thus leads to chaos.

The phase space ($\tau_d = 12, m = 5$) and the Poincaré plane clearly show the structure of the broken torus that belongs to this chaotic state. The importance of the Poincaré section is revealed here, as we notice how the circular structures in the quasi-periodic case, Fig. 3, become irregular in the chaotic case. The Poincaré section in Fig. 4 shows the deformed torus that results from torus breakdown. General features of the previously stable quasi-periodic torus can still be identified in the Poincaré plane. Note that while the phase space projections in Figs. 3 and 4 look similar, the inner structure of the attractor and the breakdown of the quasi-periodic torus becomes clear only in the corresponding Poincaré sections.

As an interim summary, Fig. 5 indicates the bifurcations identified in the system through a waterfall frequency spectra plot. Although the frequency spectra cannot be used as a tool for the diagnostics of nonlinear dynamics, it can be reinspected in the light of the results from the nonlinear analysis. In the following, further characterization of the attractors is conducted to distinguish the different states and establish the scenario observed in the thermoacoustic system.

D. Dimension estimates

The results discussed above and the inferences about the dynamical states and the bifurcation scenario are based on estimates of the correlation dimension and maximal Lyapunov exponent calculations (Sec. IV F) obtained from the reconstructed phase space trajectory. The correlation dimension is obtained by calculating the number of pairs of points on the reconstructed attractor that are spatially separated by less than ϵ, $C(\epsilon)$, while successively increasing the threshold, ϵ. The correlation dimension which is an inherent property of distinct attractors representing asymptotic dynamics of dynamical systems, is given by $\mathbf{D}_2$ satisfying the relation,

$$C(m, \epsilon) \propto \epsilon^{\mathbf{D}_2} \tag{7}$$

in the limit of $\epsilon \to 0$. The relation is satisfied in a range of ϵ values. In this range, a robust estimate of $\mathbf{D}_2$ can be found. The scaling region and the dimension estimate should be evaluated for several embedding dimensions, m, before coming to a consistent conclusion. To avoid effects of temporal correlation[40] on $\mathbf{D}_2$ calculations, only points that are separated in time by more than 120 datapoints have been considered.

Figures 6 present the variation of $C(\epsilon)$ with respect to ϵ for the distinguishing cases in the current study for several values of the embedding dimension, m. In the scaling range, the slope between $log(C)$ and $log(\epsilon)$, denoted here by $\mathfrak{D}$, becomes independent of m and ϵ. For different cases, we have identified scaling regions that are roughly around $\epsilon/D \sim 0.2$–0.3. Here D is a measure of the attractor diameter. For the determination of $\mathbf{D}_2$, we plot the variation of the slope of $\log(C)$ vs. $\log(\epsilon)$ curves, $\mathfrak{D}(m, \epsilon)$ (Fig. 6-8). For each case, the scaling region is clearly observed in these plots.

Before discussion the specific cases, if we look at the general trend of the variation of $\mathfrak{D}$ with $\log(\epsilon)$: at low

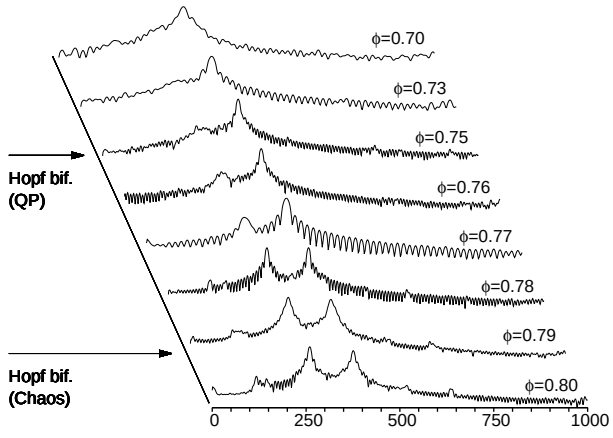

FIG. 5. Frequency bifurcation plot indicating the bifurcations of the system from limit cycle to chaos via the Ruelle-Takens scenario.

ϵ, the curves fluctuate strongly about a high value of $\mathfrak{D}$, followed by a monotonous decrease till a plateau and decrease subsequently to zero. The strong fluctuations at low ϵ are due to the finite length of data[41]. The relatively high values of $\mathfrak{D}$ at low ϵ are due to noise in the data[41,42]. It can be noticed that $\mathfrak{D}$ starts around the embedding dimension used for the calculations. As $\mathfrak{D}$ is increased, $\mathfrak{D}$ approaches the actual dimension of the attractor. The plateau is the scaling region where $\mathfrak{D}$ corresponds to the dimension of the system.

The cases identified as to correspond to a limit cycle have a correlation dimension of $\mathbf{D}_2 \sim 1.56$. This is consistent with the geometrical property of a limit cycle. The limit cycle has a geometrical dimension of 1. The calculated non-integer value, 1.56, could originate from the following sources: the fractal nature of the attractor and effect of noise[42]. We propose that for the cases investigated, non-additive noise arising from fluctuation of system parameters is responsible for increasing the observed $\mathbf{D}_2$ value.

For the quasi-periodic cases, $\phi \in [0.75, 0.79)$, the dimension, $\mathbf{D}_2 \sim 2.5$. Again considering this attractor is not chaotic (Sec. IV F) and that noise causes an increase in the calculated dimension, the results conforms with the properties of a two-torus, which in the noise-free case would have a geometrical dimension of two. The effect of noise is also seen in the Poincaré section in Fig. 3, where the blurred torus rings are seen instead of the distinct ring expected from a two-torus.

As this torus breaks, the attractor dimension jumps to a higher value of $\mathbf{D}_2 \sim 3.6$. The confirmation that this attractor is chaotic comes from the calculation of the maximal Lyapunov exponent in Sec. IV F. Chaotic attractors are often fractal structures[29]. Hence, it is likely that the non-integer value of $\mathbf{D}_2$ indicates a strange chaotic attractor. In addition, the effect of noise should also be taken into consideration.

E. Sources of noise

In the turbulent flame combustor investigated, the highly unsteady nature of the turbulent flame plays a major role in the generation of noise that affects dynamical characteristics of the system (i.e. noise is not just additive). Added to the inherently turbulent nature of the flame, in complex systems such as the considered turbulent combustor, it is difficult to maintain a strictly constant condition. Therefore unavoidable changes in critical system parameters occur during the experiments. These parameter changes can directly or indirectly affect properties of the flame and, in general, may modulate contribution from other physical mechanisms, such as hydrodynamic instabilities, involved in the thermoacoustic coupling. Hence, they can affect thermoacoustic coupling; we can assume that the property changes are not so significant as to induce abrupt dynamical changes such as bifurcations. However, the modulations induced due to these expected fluctuations can ultimately affect estimates of dynamical invariants such as $\mathbf{D}_2$. The situation is clearly different from the previously investigated laminar flame systems[23], but pertains more to practical applications such as gas-turbine combustors. Despite these constraints, estimates of dynamical invariants could be obtained in our case, thus, enabling us to identify bifurcations in the system.

F. Estimates of the Lyapunov exponent

Finally, in this section, we report the estimates of the maximal Lyapunov of the different cases discussed in earlier sections. The Lyapunov estimates support the bifurcation scenario elaborated in Secs. IV A-IV C. More specifically, we present Lyapunov calculations supporting the observation that beyond $\phi = 0.77$, the system is governed by chaotic dynamics emerging from the torus breakdown. Fig. 9 presents the variation of the average

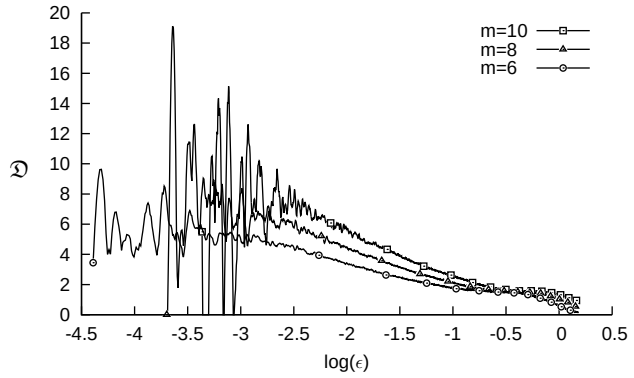

FIG. 6. Representative correlation dimension calculations for $\phi \in [0.70 - 0.75)$. In the scaling region, the dimension is estimated to be around $\mathbf{D}_2 \sim 1.56$.

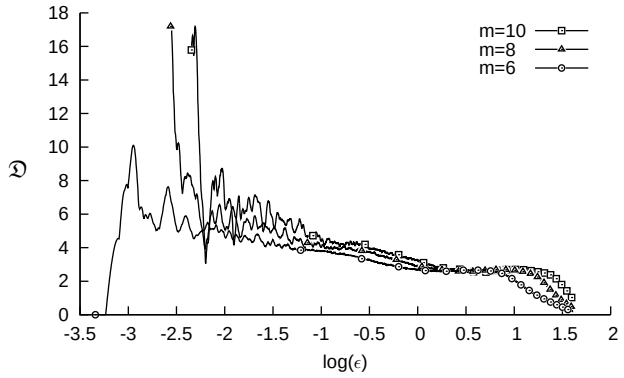

FIG. 7. Representative correlation dimension calculations for $\phi \in [0.75, 0.79)$. In the scaling region, the dimension is estimated to be around $\mathbf{D}_2 \sim 2.5$.

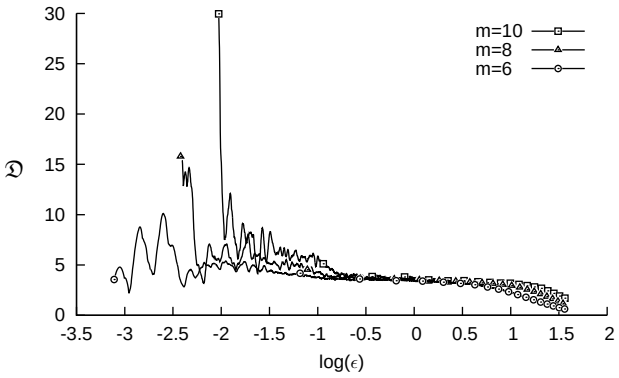

FIG. 8. Representative correlation dimension calculations for $\phi = 0.79, 0.80$. In the scaling region, the dimension is estimated to be around $\mathbf{D}_2 \sim 3.6$.

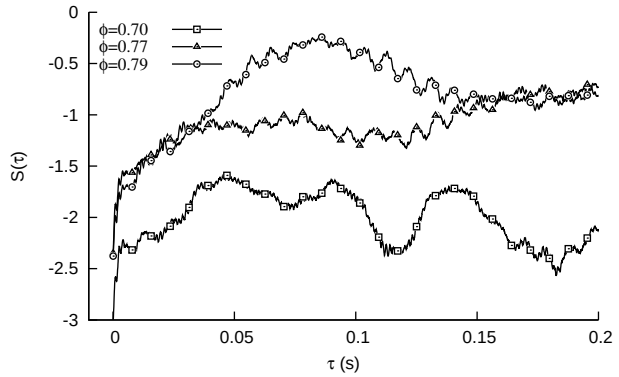

FIG. 9. λ_{max} calculations for the three representative cases.

divergence of trajectories $S(\tau)$, specifically, with time, τ. The calculations follow those reported in Ref. 30 for the estimation of the maximal Lyapunov exponent. While the limit cycle and quasi-periodic cases do not show a pronounced slope, a distinct positive slope is clear in the case that we identified to be chaotic. The pronounced positive slope for the chaotic case is a confirmation of the divergence of close-by trajectories. The value of the positive slope gives the estimate of the maximum exponential divergence of the neighboring trajectories. For our chaotic case, the value obtained for the maximal Lyapunov exponent, λ_{max}, is found to be $\lambda_{max} = 18.9 \pm 0.1$.

V. CONCLUSIONS

The article reports a series of analyses on nonlinear thermoacoustic oscillations. The specific contribution of this report is to show the presence of a standard bifurcation scenario in a practically relevant combustor configuration. We analysed the various nonlinear states resulting from successive bifurcations through analysis in the time domain, frequency domain and in the reconstructed phase space. The sequence of changes observed in the experiments are as follows: 1) with the introduction of an incommensurate frequency, the limit cycle undergoes transition to quasi-periodicity; 2) the new incommensurate frequency grows in amplitude as the bifurcation parameter is varied further; and 3) a small contribution from a third incommensurate frequency results in a distorted phase space attractor. The resulting could either be a noisy quasi-periodic attractor with three incommensurate frequencies or a chaotic attractor[38]. Through characterization of the nonlinear states via correlation dimension and Lyapunov exponent estimates, we found that the final state corresponds to a chaotic, and possibly strange, attractor. Hence, the system exhibits a Ruelle-Takens scenario in its transition from limit cycle oscillations to low-dimensional, deterministic chaos. This scenario is consistent with recent studies. This is an encouraging result emerging from the experimental study of a system that contains most of the important features and complexities of a real combustor.

It is expected that the observed nonlinear bifurcations arise as a result of the nonlinear behavior of the technically-premixed flame. With the global equivalence ratio as the control parameter, the observed spectrum of nonlinear dynamics of thermoacoustic oscillations can clearly be inferred to be a result of critical variations in flame dynamics with varying equivalence ratio. Therefore, the criticality of an appropriate treatment of the nonlinear flame dynamics for improved modeling and control of thermoacoustic oscillations emerges as an important message from the presented experiments and the nonlinear analysis of the data.

ACKNOWLEDGMENTS

The experimental part of this work was funded by the EU project IMPACT AE FP7-265586. Lipika Kabiraj would like to acknowledge the German Research Foundation for financially supporting her research at the Technische Universität Berlin (grant no. KA 3968/1-1). Anna Sailor would like to thank the DAAD for supporting her research internship at the Technische Universität Berlin.

[1] T. C. Lieuwen and V. Yang, Progress in astronautics and aeronautics (2005).
[2] S. Candel, Proceedings of the Combustion Institute **29**, 1 (2002).
[3] Rayleigh, Nature **18**, 319 (1878).
[4] T. Sattelmayer, Journal of Engineering for Gas Turbines and Power **125**, 11 (2003).
[5] T. Lieuwen, Y. Neumeier, and B. Zinn, Combustion Science and Technology **135**, 193 (1998).
[6] T. C. Lieuwen, *Unsteady combustor physics* (Cambridge University Press, 2012).
[7] Y. Huang and V. Yang, Progress in Energy and Combustion Science **35**, 293 (2009).
[8] K. T. Kim, J. G. Lee, B. D. Quay, and D. A. Santavicca, Combustion and Flame **157**, 1731 (2010).
[9] B. C. Bobusch, B. Ćosić, J. P. Moeck, and C. O. Paschereit, Journal of Engineering for Gas Turbines and Power **136**, 021506 (2014).
[10] T. Lieuwen and B. T. Zinn, Symposium (International) on Combustion **27**, 1809 (1998).

[11]N. Karimi, Energy (2014), doi:10.1016/j.energy.2014.10.036.
[12]N. Karimi, M. J. Brear, S.-H. Jin, and J. P. Monty, Combustion and Flame **156**, 2201 (2009).
[13]T. Schuller, D. Durox, and S. Candel, Combustion and Flame **134**, 21 (2003).
[14]A. P. Dowling and S. R. Stow, Journal of Power and Propulsion **19**, 751 (2003).
[15]A. P. DOWLING, Journal of Fluid Mechanics **346**, 271 (1997).
[16]D. Durox, T. Schuller, N. Noiray, and S. Candel, Proceedings of the Combustion Institute **32**, 1391 (2009).
[17]N. Noiray, D. Durox, T. Schuller, and S. Candel, Journal of Fluid Mechanics **615**, 139 (2008).
[18]R. Balachandran, B. Ayoola, C. Kaminski, A. P. Dowling, and E. Mastorakos, Combustion and Flame **143**, 37 (2005).
[19]K. Ogata, *Modern Control Engineering* (Prentice-Hall, 1970).
[20]S. Hemchandra, Combustion and Flame **159**, 3530 (2012).
[21]Shreekrishna, S. Hemchandra, and T. Lieuwen, Combustion Theory and Modelling **14**, 681 (2010).
[22]A. Birbaud, S. Ducruix, D. Durox, and S. Candel, Combustion and Flame **154**, 356 (2008).
[23]L. Kabiraj, A. Saurabh, and R. I. Sujith, Chaos: An Interdisciplinary Journal of Nonlinear Science **22**, 023129 (2012).
[24]H. Gotoda, H. Nikimoto, T. Miyano, and S. Tachibana, Chaos **21**, 013124 (2011).
[25]L. Kabiraj, *Intermittency and Route to Chaos in Thermoacoustic Oscillations*, Ph.D. thesis, Indian Institute of Technology, Madras (2012).
[26]V. Nair and R. I. Sujith, Proceedings of Combustion Institute (2014), doi:10.1016/j.proci.2014.07.007.
[27]K. Kashinath, *Nonlinear thermoacoustic oscillations of a ducted premixed laminar flame*, Ph.D. thesis, University of Cambridge, Cambridge, UK (2013).
[28]S. H. Strogatz, *Nonlinear Dynamics and Chaos: With Applications to Physics, Biology, Chemistry and Engineering* (Westview Press, 2000).
[29]H. Abarbanel, B. R., J. Sidorowich, and L. Tsimring, Reviews of Modern Physics **65**, 1331 (1993).
[30]H. Kantz, Physics Letters A **185**, 77 (1994).
[31]Subscript two denotes that correlation dimension corresponds to the generalized dimension of order two.
[32]P. Grassberger and I. Procaccia, Physical Review Letter **50**, 346 (1983).
[33]H. Kantz and T. Schreiber, *Nonlinear Time Series Analysis* (Cambridge Press, 2003).
[34]C. C. Jahnke and F. E. C. Culick, Journal of Propulsion and Power **10**, 508 (1994).
[35]I. Matveev, *Thermo-acoustic instabilities in the Rijke tube: experiments and modeling*, Ph.D. thesis, CalTech, Pasadena, CA (2003).
[36]L. Kabiraj and R. I. Sujith, Journal of Fluid Mechanics **713**, 376 (2012).
[37]N. Karimi, E. Mastorakos, and A. P. Dowling, in *Proceedings of the 6th European Combustion Meeting*, P3-24 (Lund, Sweden, 2013) p. 6pp.
[38]A. Nayfeh and B. Balachandran, *Applied Nonlinear Dynamics: Analytical, Computational and Experimental Methods*, Wiley Series in Nonlinear Science (2008).
[39]R. Hilborn, *Chaos and Nonlinear Dynamics: An Introduction for Scientists and Engineers* (Oxford University Press, USA, 2001).
[40]J. Theiler, Phys. Rev. A **34**, 2427 (1986).
[41]T. Schreiber, Physics Reports **308**, 1 (1999).
[42]H. Kantz and T. Schreiber, Chaos: An Interdisciplinary Journal of Nonlinear Science **5**, 143 (1995).